Journal of Cardiovascular Computed Tomography 14 (2020) 149–154

Contents lists available at ScienceDirect

Journal of Cardiovascular Computed Tomography

journal homepage: www.elsevier.com/locate/jcct

Research paper

Validation of a computational model aiming to optimize preprocedural planning in percutaneous left atrial appendage closure

Alessandra M. Bavo[a,*], Benjamin T. Wilkins[b], Philippe Garot[c], Sander De Bock[a], Jacqueline Saw[d], Lars Søndergaard[b], Ole De Backer[b], Francesco Iannaccone[a]

[a] FEops NV, Ghent, Belgium
[b] The Heart Centre, Rigshospitalet, Copenhagen, Denmark
[c] Hôpital Privé Jacques Cartier, Institut Cardiovasculaire Paris Sud (ICPS), Ramsay-Générale de santé, Massy, France
[d] Division of Cardiology, Vancouver General Hospital, University of British Columbia, Vancouver, Canada

ARTICLE INFO

Keywords:
Atrial fibrillation
Percutaneous left atrial appendage closure
CCT-based computational model
Patient-specific anatomy
Pre-operative planning

ABSTRACT

Background: Percutaneous left atrial appendage (LAA) closure can be optimised through diligent preprocedural planning. Cardiac computational tomography (CCT) is increasingly recognised as a valuable tool in this process. A CCT-based computational model (FEops HEARTguide™, Belgium) has been developed to simulate the deployment of the two most commonly used LAA closure devices into patient-specific LAA anatomies.
Objective: The aim of this study was to validate this computational model based on real-life percutaneous LAA closure procedures and post-procedural CCT imaging.
Methods: Thirty patients having undergone LAA closure (Amulet™ n = 15, Watchman™ n = 15) and having a pre- and post-procedural CCT-scan were selected for this validation study. Virtually implanted devices were directly compared to actual implants for device frame deformation and LAA wall apposition.
Results: The coefficient of determination (R^2) and the difference in measurements between model and actual device (area, perimeter, minimum diameter, maximum diameter) were ≥0.91 and ≤ 5%, respectively. For both device types, the correlation coefficient between predicted and observed measurements was higher than 0.90. Furthermore, predicted device apposition correlated well with observed leaks based on post-procedural CCT.
Conclusion: Computational modelling accurately predicts LAA closure device deformation and apposition and may therefore potentiate more accurate LAA closure device sizing and better preprocedural planning.

1. Introduction

Percutaneous left atrial appendage (LAA) closure is being increasingly used as a treatment strategy to prevent stroke in patients with non-valvular atrial fibrillation (NVAF) and contra-indication(s) to oral anticoagulant therapy. In order to obtain a successful LAA closure, accurate LAA closure device size selection as well as optimal implantation should be aimed for. The official instructions for use and sizing charts for all approved LAA closure devices are still based on 2D transesophageal echocardiographic (TEE) measurements. However, in parallel with the transcatheter aortic valve replacement (TAVR) field, an increasing number of centers have recently shifted towards LAA sizing based on cardiac computed tomography (CCT) imaging. Although this more accurate pre-procedural imaging definitely helps to better understand and size the patient's LAA anatomy, predicting the actual 'landing zone' of the LAA closure device still remains difficult and an important source of sizing error. The use of a computational model simulating different LAA closure devices, device sizes and implant positions may be helpful in the preprocedural planning of these procedures. This study aims to validate these computational models and simulations, based on real-life percutaneous LAA closure procedures and post-procedural CCT imaging.

2. Methods

2.1. Study population

Thirty patients who had undergone percutaneous LAA closure with an Amplatzer Amulet (Abbott, MN, USA; N = 15) or Watchman (Boston Scientific, MA, USA; N = 15) LAA occluder and who had pre- and post-procedural CCT-scans available were retrospectively selected for this study. Patients were treated in three different centers: Institut

* Corresponding author. FEops NV, Technologiepark 122, 9052, Ghent, Belgium.
E-mail address: alessandra.bavo@feops.com (A.M. Bavo).

https://doi.org/10.1016/j.jcct.2019.08.010
Received 12 April 2019; Received in revised form 1 July 2019; Accepted 19 August 2019
Available online 20 August 2019
1934-5925/

Abbreviations

LAA	left atrial appendage
CCT	cardiac computational tomography
NVAF	non-valvular atrial fibrillation
TEE	transesophageal echocardiographic
TAVR	transcatheter aortic valve replacement
CAD	computer aided design
Dmin	minimum diameter
Dmax	maximum diameter

Cardiovasculaire Paris Sud (France), Rigshospitalet – Copenhagen University Hospital (Denmark), and Vancouver General Hospital (Canada). All CCT-scans were ECG-gated, contrast-enhanced and with thin slice thickness (0.5–1.0 mm). Post-procedural CCT scans were acquired 1–12 months after the procedure.

2.2. Computational modelling

Computational models of all sizes of the Amulet and Watchman LAA closure devices were built on the FEops HEARTguide™ platform (FEops NV, Ghent, Belgium) with a reverse engineering approach, where a known reference surface representation of the device is used to generate the model. The reference surface to generate the Amulet devices was reconstructed from a micro-CT scan of the device, while for the Watchman device the CAD (computer aided design) data provided by the manufacturer were used. Experimental bench testing performed on the devices served to calibrate the stiffness of the computational models. To generate the patient-specific geometry, the pre-operative CCT data were segmented by use of Mimics software v21.0 in order to extract the 3D surface of the left atrium. The geometry was limited to the LAA region including, at minimum, the left atrium and the origin of the pulmonary veins (Fig. 1A and B). The stiffness of the LAA was determined after calibration on a pool of 15 patients implanted with an Amulet device, not included in this study. The computer-generated LAA closure devices were virtually implanted into the patient-specific anatomy using finite-element computational simulation, allowing to predict both device and tissue deformation. All simulations were performed using the Abaqus/Explicit finite element solver v17.0 (Dassault Systems, Paris, France). The device implant position was matched with the actual device position by visual comparison between the numerical results and the post-procedural CCT reconstructed geometry (Fig. 1C and D).

2.3. Measurement of device frame deformation

The geometry of the implanted device and the left atrium were extracted from the post-operative images. The difference in device frame deformation between the observed (post-operative CCT scan) and predicted (computational model) results was measured and calculated. The device frame deformations were quantified at a single predefined section of the device. As the design of the Amulet and Watchman closure devices are profoundly different, different locations for the measurements were identified. For the Amulet device, the mid-cross section of the lobe was extracted, and its area, perimeter, maximum diameter (Dmax) and minimum diameter (Dmin; perpendicular to Dmax) were measured. For the Watchman device, the largest section of the device was identified, fitted with a curve, and its area, perimeter, Dmax and Dmin (perpendicular to Dmax) were measured. The section identification and measurements were performed automatically and were thus not influenced by operator variability.

2.4. Wall apposition

From the computational models, the distance between the closure device and the LAA wall can be measured. For both devices, the distance to the nearest atrial surface are presented as a colour-plot, where white corresponds to complete wall apposition, whereas red indicates a distance of at least 2 mm between the device and the nearest LAA wall. For the Watchman device, the distance was plotted on the membrane sewn on the device, while for the Amulet device, the distance was plotted on a fictitious surface wrapped around the device.

A qualitative evaluation was performed to classify whether or not the computational model predicts a peri-device leak. For the Amulet devices, having a good predicted sealing on either the disc or the lobe (or both) is associated with full closure of the LAA. On the contrary, having large areas with a distance greater than 2 mm or multiple gaps on the disc and/or the lobe can be considered as a poorly closed LAA. For Watchman devices, the presence of full channels passing along the membrane or extended gaps at the shoulders level were considered as poorly closed LAAs. This qualitative evaluation of the predicted sealing/leak was then compared with the observed leaks based on the post-operative CT scan. For the latter, a binary classification was used, where 0 indicates the absence of contrast in the LAA and 1 represents a significant amount of bright contrast in the LAA.

2.5. Statistical analysis

Data are presented as mean ± standard deviation. Paired comparison between the observed and the predicted measurements were obtained using a paired Student's T test or the Wilcoxon signed-rank test, as appropriate. To evaluate the accuracy of the computational model predictions, the coefficient of determination (R^2) was calculated for all measurements, evaluating the difference between the predicted and the observed measurements. A coefficient of determination > 0.90 indicates good agreement between the compared measurements. Difference plots were constructed according to the Bland-Altman method. A minimum sample size of 14 patients for this validation was required.

The sample size calculation was performed assuming an alpha level error of 5%, and a statistical power of 80% (or beta error of 20%). For

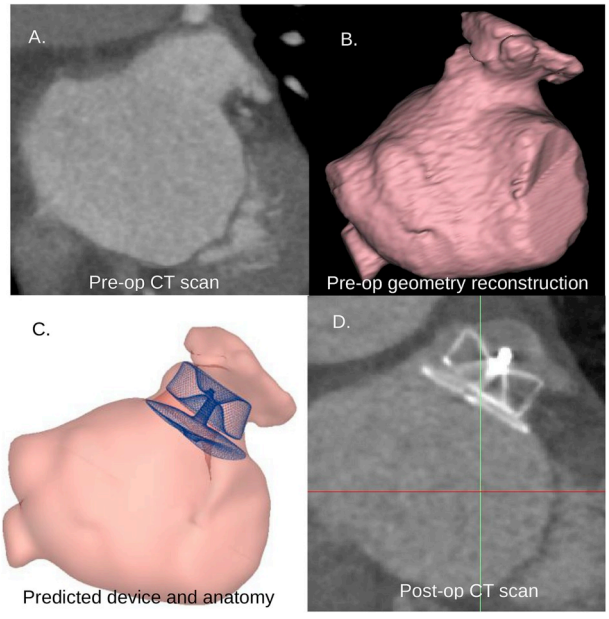

Fig. 1. Workflow: (A) pre-operative CT scan, (B) geometry reconstruction from CT scan. (C) Virtually deployed device in the anatomy and (D) post-operative CT scan used for validation.

the deployed device geometry, the assumptions for the sample size calculation are based on a calibration study, which was conducted prior the validation on an independent cohort of patients:

- Expected difference between the predicted and observed device geometry, quantified by the mean diameter at the selected location: -0.42 ± 1.0 mm.
- Maximum allowed difference between the predicted and observed device geometry ± 4.0 mm.

The maximum allowed difference corresponds to a 16% error in case of a 25 mm measurement.

3. Results

Baseline characteristics of the study population are summarized in Table 1. Different LAA closure device sizes were included in this study. As the data was collected retrospectively, some periprocedural information is missing. The number of devices used is known for 26 patients, in two of them two different device sizes were used (7%). The number of recaptures is known for 20 patients. In 8 cases, no recapture was required (40%), in 9 patients one recapture of the device was needed (45%) and in three cases more than two recaptures were performed (15%), with a maximum of 4 recaptures in one patient.

Fig. 2 shows the visual comparison for two representative patients included in this study, one treated with the Amulet device and one treated with the Watchman device. The observed (Fig. 2A and E) and predicted (Fig. 2B and F) device frame deformation are shown for both devices, the sections selected for measurements are shown in Fig. 2C and G, while the overlay of the sections are shown in Fig. 2D and H. Visual comparison was performed for all simulated cases in order to verify that the predicted device implant position corresponded to the observed postoperative implant position.

The mean and standard deviations of the observed and predicted LAA closure device dimensions (area, perimeter, Dmin, Dmax) are reported in Table 2. The coefficient of determination R^2 and the difference in measurements between model and post-operative CT-scan were calculated and were ≥ 0.91 and less than 5%, respectively. Scatter plots for Dmin and Dmax measured at the selected sections for the two device types are shown in Fig. 3A and B. For both device types, the coefficient of determination was higher than 0.90, showing a good match between the observed and the predicted frame deformation. The coefficient of determination for all measurements in the entire cohort was ≥ 0.92. Bland-Altman plots of the mean difference between the observed and predicted measurements are shown in Fig. 3C and D. No difference in the model effectiveness was found when stratifying the patients by appendage morphology.

The computational model allows to report the apposition between LAA closure device and LAA wall in an instructive, visual format. In Fig. 4, two examples of patients virtually implanted with an Amulet (upper panels) and Watchman (lower panels) LAA closure device depict the distance plot between the device and the LAA wall. Different sizes and implantationd depths of the device can be simulated. The evaluation of the leaks predicted by the model was blindly performed by two independent operators. The comparison between the predicted device leaks and the actual contrast leak detected on post-operative CT scans resulted in an accuracy, sensitivity, specificity, positive predicted value and negative predicted value of 77%, 71%, 81%, 77% and 76% respectively.

4. Discussion

Percutaneous LAA closure prevents blood flow to and from the LAA, a cardiac structure where 90% of thrombi in patients with NVAF is suspected to originate.[1] In order to improve procedural outcomes, optimal LAA imaging and sizing is essential. Undersizing of the device may lead to incomplete closure or even device embolization, while oversizing may cause tamponade, device embolization or late erosion. CCT scanning is increasingly recognised as a powerful tool in the planning of LAA closure,[2] and allows for detailed models to be

Table 1
Baseline characteristics

FEops ID	Age/Sex	BMI	CHA 2 DS 2 -Vasc	HAS-BLED	LAA morphology	LAA ostium	LAA landing zone	Device type	Device size	Post-op CT leaks
LAA0040	83/F	36.3	5	2	Windsock	16.4 × 17.9	12.4 × 18.1	Amulet	18	0
LAA0042	71/M	27.7	4	3	Windsock	19.0 × 24.9	13.5 × 19.6	Amulet	20	0
LAA0046	74/F	24.5	2	1	Chicken wing	22.0 × 27.1	19.2 × 21.8	Amulet	22	0
LAA0053	74/M	27.8	4	3	Chicken wing	22.0 × 29.4	14.2 × 23.2	Amulet	22	1
LAA0055	73/F	37	4	3	Cactus	16.4 × 25.3	15.4 × 28.7	Amulet	22	1
LAA0056	78/F	19.8	6	3	Windsock	19.3 × 25.2	17.7 × 24.0	Amulet	22	0
LAA0057	78/F	19.6	5	2	Chicken wing	16.0 × 24.7	17.0 × 24.6	Amulet	22	1
LAA0025	80/M	21.8	3	2	Chicken wing	21.0 × 28.4	18.7 × 25.2	Amulet	25	0
LAA0099	85/M	24.2	4	3	Windsock	31.1 × 35.5	20.9 × 22	Amulet	25	1
LAA0105	74/F	18.1	4	4	Chicken Wing	19.4 × 24.6	19.5 × 26.2	Amulet	25	1
LAA0026	65/M	20	2	2	Windsock	27.6 × 35.3	22.6 × 25.0	Amulet	28	0
LAA0039	64/F	23.5	2	2	Chicken wing	18.4 × 28.6	23.6 × 26.7	Amulet	28	1
LAA0063	73/M	25.8	2	3	Chicken wing	20.0 × 30.5	19.5 × 29.2	Amulet	28	1
LAA0067	86/M	21.4	5	3	Windsock	26.9 × 36.8	24.6 × 32.8	Amulet	31	0
LAA0080	83/M	23.9	5	4	Cauliflower	31.0 × 50.3	28.9 × 37.0	Amulet	34	0
LAA0048	73/F	33.4	4	2	Windsock	18.6 × 25.2	N.A.	Watchman	21	1
LAA0092	81/M	31	5	5	Windsock	15.8 × 25.5	N.A.	Watchman	21	0
LAA0095	83/M	25.3	3	3	Windsock	21.6 × 22.6	N.A.	Watchman	21	0
LAA0001	70/M	23.5	4	4	Chicken wing	17.5 × 27.6	N.A.	Watchman	24	0
LAA0002	73/F	22.6	7	3	Chicken wing	19.8 × 27.5	N.A.	Watchman	24	0
LAA0011	71/M	26.5	4	3	Windsock	19.6 × 25.0	N.A.	Watchman	24	0
LAA0091	78/M	25.6	2	1	Windsock	17 × 24.2	N.A.	Watchman	24	1
LAA0103	85/M	28.1	4	5	Chicken wing	18.2 × 25	N.A.	Watchman	24	1
LAA0047	80/F	29	5	3	Windsock	24.4 × 31.6	N.A.	Watchman	27	0
LAA0061	68/M	31.9	3	3	Windsock	24.6 × 27.5	N.A.	Watchman	27	0
LAA0069	82/M	23.5	4	2	Chicken wing	19.6 × 30.9	N.A.	Watchman	30	1
LAA0102	79/M	20.8	4	5	Windsock	24.1 × 29.9	N.A.	Watchman	30	1
LAA0119	83/M	31.2	3	4	Windsock	32.8 × 48.2	N.A.	Watchman	30	0
LAA0113	79/M	31.4	5	4	Chicken Wing	25.3 × 32.5	N.A.	Watchman	33	1
LAA0117	83/F	15.2	6	4	Chicken Wing	23.5 × 33.6	N.A.	Watchman	33	1

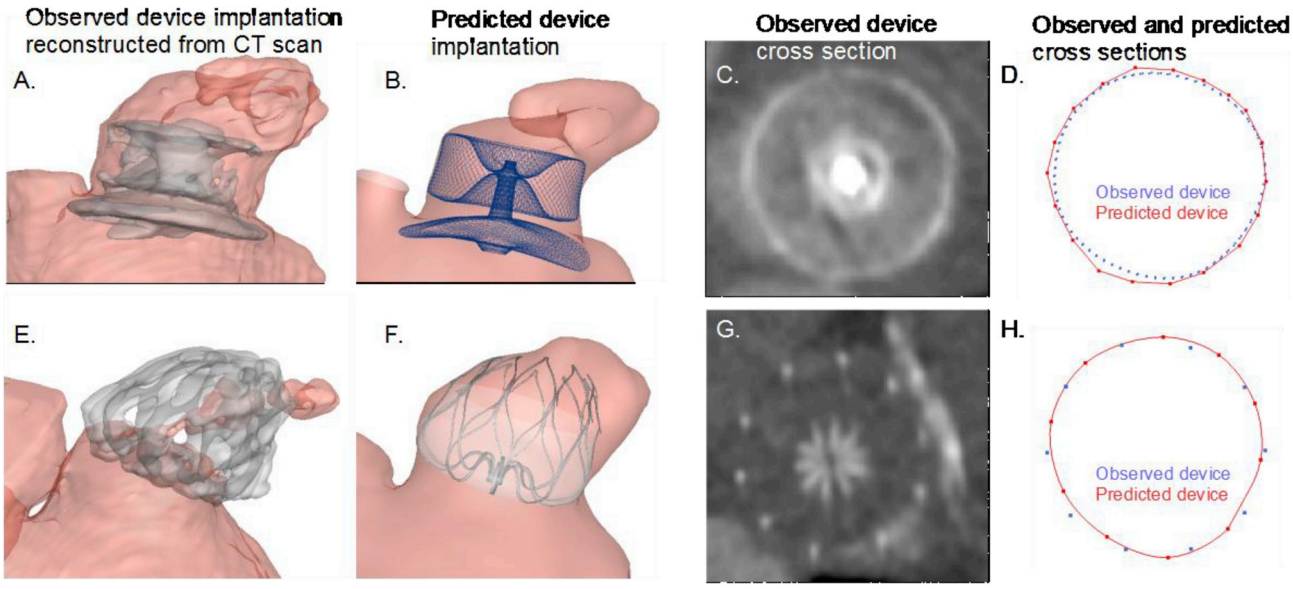

Fig. 2. Visual comparison between observed and implanted device position for Amulet (A-D) and Watchman devices (E-H).

Table 2
Comparison of device deformation measurements

	CCT	Model	Coefficient of Determination R^2 [-]	Difference Model - CCT
Amulet (N = 15)				
Area [mm2]	437.4 ± 163	445.6 ± 177	0.96	15.0 ± 44.7 (p-value = 0.22)
Perimeter [mm]	73.4 ± 13.4	74.5 ± 13.8	0.96	0.7 ± 3.6 (p-value = 0.45)
Dmin [mm]	22.6 ± 4.0	23.0 ± 4.2	0.95	0.3 ± 1.3 (p-value = 0.33)
Dmax [mm]	24.0 ± 4.5	24.3 ± 4.5	0.95	0.1 ± 1.2 (p-value = 0.64)
Watchman (N = 15)				
Area [mm2]	470.1 ± 155	481 ± 160	0.94	14.5 ± 36.0 (p-value = 0.14)
Perimeter [mm]	76.35 ± 11.7	76.9 ± 12.4	0.92	1.0 ± 2.9 (p-value = 0.19)
Dmin [mm]	23.7 ± 3.7	23.9 ± 3.9	0.91	0.3 ± 0.9 (p-value = 0.19)
Dmax [mm]	24.95 ± 3.8	25.0 ± 3.9	0.92	0.3 ± 1.1 (p-value = 0.29)
Total cohort (N = 30)				
Area [mm2]	453.7 ± 160	468 ± 169	0.95	14.8 ± 39.2 (p-value = 0.045)
Perimeter [mm]	74.8 ± 12.7	75.7 ± 13.1	0.94	0.9 ± 3.2 (p-value = 0.15)
Dmin [mm]	23.1 ± 3.9	23.5 ± 4.1	0.92	0.3 ± 1.1 (p-value = 0.11)
Dmax [mm]	24.5 ± 4.2	24.7 ± 4.3	0.94	0.2 ± 1.1 (p-value = 0.28)

generated.

As an interventional target, the LAA has considerably more anatomic variation than other cardiac structures, which may increase the procedure complexity.[3] Computational models can provide physicians additional insights into patient-specific anatomy and its interaction with the implanted device. This study demonstrated as a first that patient-specific computational modelling allows accurate prediction of LAA closure device deformation.

The development and use of an accurate predictive simulator for percutaneous LAA closure may have important clinical relevance. As shown in Table 2**,** there was less than 0.3 mm (2%) difference in Dmin between FEops HEARTguide™ simulated and actual implants and a difference of less than 0.2 mm (1.5%) for Dmax measurements. The differences between observed and predicted frame deformation are not statistically significant for all the analyzed quantities, with the exception of the area measurements of the full cohort of patients. None of the absolute differences measured is clinically relevant for the application of interest. Furthermore, as a device compression rate of 15%–25% is typically aimed for, this difference between simulated and observed measurements can be considered acceptable and within the compression tolerance of LAA closure devices.

Semi-quantitative apposition plots of the implanted closure device can help in predicting the potential risk for peri-device leaks. The correspondence between post-operative leaks and presence of incomplete device sealing based on the simulation results is promising, suggesting a good predictive power of the computational model for peridevice leaks.

The model allows for implantation at a range of depths, giving the ability to observe detailed LAA-device interactions. Optimized device size selection and implantation by use of computational modelling may allow for a reduction in the commonly observed peri-device leaks, seen in 20%–40% of cases at post-procedural LAA closure imaging.[4,5] At present, there is no hard evidence showing that peri-device leak is associated with an increased risk of stroke. However, patients with incomplete closure are more likely to remain on anticoagulants,[4] negating the need for LAA closure for many patients. In addition, there remains a high suspicion amongst clinicians that an incompletely closed LAA can remain thrombogenic over the patients' lifetime.

An additional strength of preoperative computational modelling may be that operators will start the procedure with a well-defined plan – instead of more 'ad hoc' decision-taking and changes under the procedure. This may not only reduce the procedural length and radiation exposure but also the inherent risks of additional catheter exchanges, atrial trauma or air embolism. In addition, this approach may reduce the overall number of LAA closure devices used, and thus procedural costs. In accordance, preprocedural planning using LAA 3D-models has

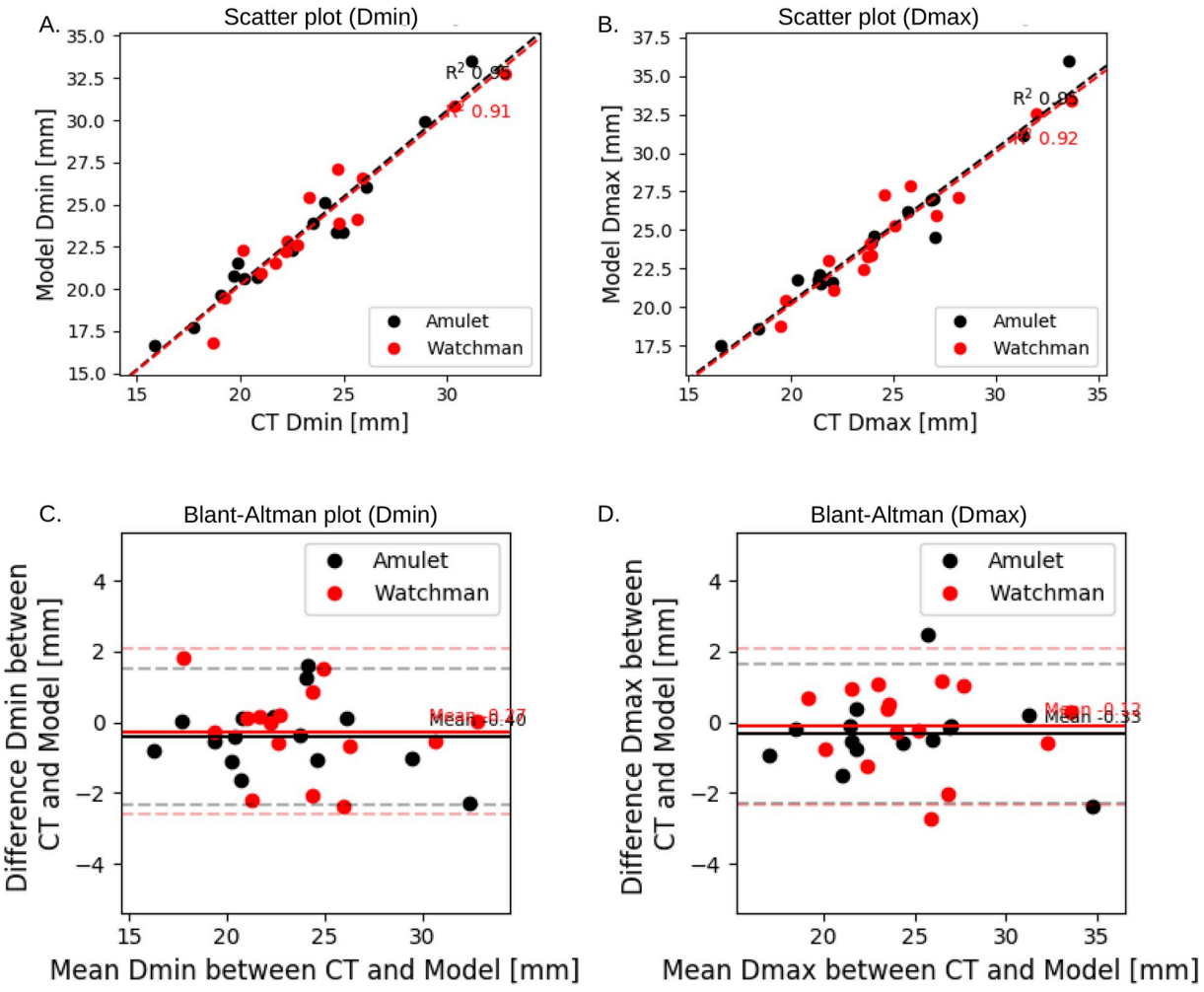

Fig. 3. (A-B) Scatter plot for minimum and maximum diameters. The results of the Amulet are reported in black, while the results of Watchman are reported in red. (C-D) Bland-Altman difference plot for minimum and maximum diameters. The results of the Amulet are reported in black, the results of Watchman are reported in red.

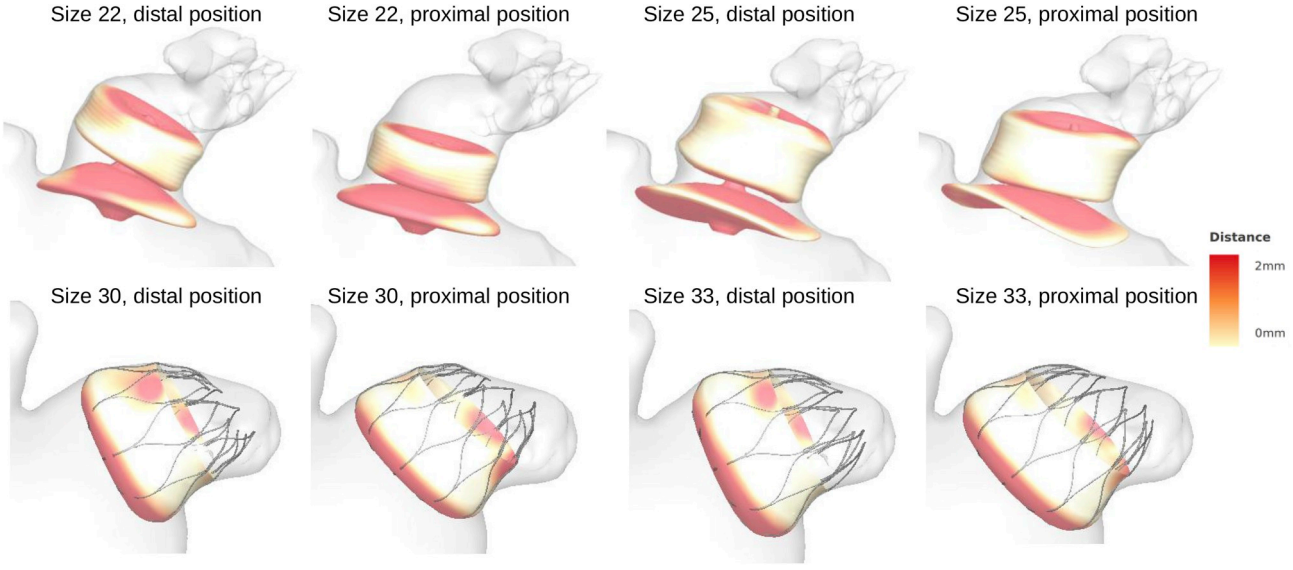

Fig. 4. Apposition plot for a patient implanted with Amulet (upper panels) and one implanted with Watchman (lower panels) devices. Different sizes and positions are virtually simulated. White corresponds to perfect apposition, while a red color indicates gaps between the device and the walls of 2mm or greater.

already been reported to significantly reduce the number of devices used per procedure as well as reduce the number of cases with remaining contrast leakage (≥grade 2) into the LAA at follow-up CCT-scan.[6]

Furthermore, it is foreseeable that accurate LAA closure device selection before the procedure may allow another set-up for this procedure. The generally accepted role for TEE to assist with device size selection and positioning could be substituted with intracardiac echo or micro TEE, converting LAA closure from a general anaesthetic to a local anaesthetic procedure.

4.1. Limitations and future perspectives

One of the possible limitations of this study is that the model was validated with post-operative CCT data ranging from 1 to 12 months after the procedure. As a result, it may not capture acute device deformation at the time of implantation. Fluoroscopy is unlikely to be a useful surrogate for any acute device deformational measurement as it is not possible to make accurate measurements on 2D images. Acquisition of post-operative CCT images early after the procedure could help to further evaluate this. Moreover, the model relies on CCT imaging of sufficient quality to allow an accurate reconstruction. CCT scans with poor contrast mixing, motion blur or artefacts in any portion of the LAA will typically have to be excluded. From an anatomical point of view, although the model can include the geometrical features of muscle bundles, it does not take into account the possible increase in wall stiffness these might introduce. Data are currently being collected to investigate and target this limitation. A final limitation may also be that the operator is not always capable of implanting the device in the position as simulated. Multiple depth positions can be modelled; however, whether operators can implant LAA closure devices accurately in a pre-specified position remains to be verified.

5. Conclusions

Computational modelling of LAA closure procedures can provide physicians additional insights to patient-specific anatomy and its interaction with implanted devices. FEops HEARTguide™ simulation provides accurate simulation of implants for the most commonly used Amulet™ and Watchman™ LAA occluders. The semi-quantitative representation offered by apposition plots of implanted devices identifies the potential presence of malapposition and peri-device leaks. A randomized controlled trial comparing standard pre-procedural planning with computational model-assisted pre-procedural planning is planned to start in 2019.

Conflicts of interest

A. M. Bavo, S. De Bock and F. Iannaccone are employees of FEops. J. Saw declares the following:

- Research: University of British Columbia Division of Cardiology, AstraZeneca, Abbott Vascular and Servier
- Consultant/advisory board: Boston Scientific, Abbott Vascular, AstraZeneca, Bayer
- Speaker honoraria: AstraZeneca, Abbott Vascular, Boston Scientific, Bayer and Sunovion
- Proctor: Boston Scientific and Abbott Vascular

B. Wilkins, P. Garot, L. Søndergaard and O. De Backer do not have conflict of interest to declare for this study.

Acknowledgement

Author B. Wilkins is supported with a research grant from the Heart Foundation of New Zealand.

References

1. Blackshear JL, Odell JA. Appendage obliteration to reduce stroke in cardiac surgical patients with atrial fibrillation. *Ann Thorac Surg.* 1996;61:755–759.
2. Rajwani A, Nelson AJ, Shirazi MG, et al. CT sizing for left atrial appendage closure is associated with favourable outcomes for procedural safety. *Eur Heart J Cardiovasc Imaging.* 2017;18(12):1361–1368. https://doi.org/10.1093/ehjci/jew212.
3. Beigel R, Wunderlich NC, Ho SY, Arsanjani R, Siegel RJ. The left atrial appendage: anatomy, function, and noninvasive evaluation. *JACC Cardiovasc Imaging.* 2014;7(12):1251–1265. https://doi.org/10.1016/j.jcmg.2014.08.009.
4. Viles-Gonzalez JF, Kar S, Douglas P, et al. The clinical impact of incomplete left atrial appendage closure with the watchman device in patients with atrial fibrillation: a PROTECT AF (percutaneous closure of the left atrial appendage versus warfarin therapy for prevention of stroke in patients with atrial fibrillation) substudy. *J Am Coll Cardiol.* 2012;59(10):923–929. https://doi.org/10.1016/j.jacc.2011.11.028.
5. Berti S, Santoro G, Brscic E, et al. Left atrial appendage closure using AMPLATZER™ devices: a large, multicenter, Italian registry. *Int J Cardiol.* 2017;248:103–107. https://doi.org/10.1016/j.ijcard.2017.07.052.
6. Bieliauskas G, Otton J, Chow DHF, et al. Use of 3-dimensional models to optimize pre-procedural planning of percutaneous left atrial appendage closure. *JACC Cardiovasc Interv.* 2017;10(10):1067–1070. https://doi.org/10.1016/j.jcin.2017.02.027.